2021 43rd Annual International Conference of the
IEEE Engineering in Medicine & Biology Society (EMBC)
Oct 31 - Nov 4, 2021. Virtual Conference

2021 43rd Annual International Conference of the IEEE Engineering in Medicine & Biology Society (EMBC) | 978-1-7281-1179-7/21/$31.00 ©2021 IEEE | DOI: 10.1109/EMBC46164.2021.9630632

Image-based Cardiac Electrophysiology Simulation through the Meshfree Mixed Collocation Method

Konstantinos A. Mountris, Manuel Doblaré, Esther Pueyo

***Abstract*— State-of-the-art solvers for *in silico* cardiac electrophysiology employ the Finite Element Method to solve complex anatomical models. While this is a robust and accurate technique, it requires a high-quality mesh to prevent its accuracy from being severely deteriorated. The generation of a good quality mesh for realistic anatomical models can be very time-consuming, making the translation to the clinics challenging, especially if we try to use patient-specific geometries.**

Aiming to tackle this challenge, we propose an image-based model generation approach based on the meshfree Mixed Collocation Method. The flexibility provided by this method during model generation allows building meshfree models directly from the image data in an automatic procedure. Furthermore, this approach allows interpreting the simulation results directly in the voxel coordinates system of the image.

We simulate electrical propagation in a porcine biventricular model with the proposed method and we compare the results with those obtained using the Finite Element Method. We conclude that the proposed method can generate results that are in good agreement with the Finite Element Method solution, alleviating the requirement of a mesh and user-input during modeling with only minimum efficiency overhead.

***Clinical relevance*— This study establishes a novel pipeline for automatic image-based meshfree modelling for *in-silico* electrophysiology that is suitable for use in a clinical setting.**

I. INTRODUCTION

Sophisticated multiscale models are nowadays widely used to simulate cardiac function in healthy and disease conditions with increasing complexity. Such models couple a system of ordinary differential equations (ODE) to describe cellular dynamics (microscale) with either the bidomain [1] or the simplified monodomain model [2] to describe the propagation of the electrical impulse in the heart (macroscale).

Commonly, the Finite Element Method (FEM) is employed to solve such models. Despite FEM popularity in research, the application in the clinics is rather limited. This is mainly due to the FEM requirement for a good-quality mesh in order to ensure good accuracy. When mesh quality is reduced, the accuracy of FEM is severely deteriorated and may lead to erroneous results. Therefore, FEM requires time-consuming preprocessing to ensure mesh quality, which does not comply with clinical time restrictions, thus posing challenges to the wide adoption of this method in the clinics.

On the other hand, meshfree methods alleviate the mesh requirement of FEM and hence may be used to solve electrophysiology models in a more suitable way for clinical applications. Different meshfree approaches have already been proposed for *in silico* electrophysiology [3], [4], [5]. Amongst them, the Mixed Collocation Method (MCM) [6] has been proven as a promising alternative for the solution of the monodomain model, demonstrating both accuracy and efficiency in good agreement with FEM. MCM rather than using a mesh, obtains the solution at each field node by evaluating meshfree approximants in a support domain around the field node. The support domain is composed of a group of support nodes in the vicinity of the field node, including itself. The inherent flexibility of meshfree model generation in MCM allows to introduce the notion of immersed grid generation, where the meshfree model is generated automatically by embedding a grid of regularly distributed nodes inside a triangular surface mesh representation of the anatomy [6].

In this work, we employ MCM to generate image-based anatomical models based on the immersed grid approach for suitable *in silico* electrophysiology in clinical applications. Meshfree models are generated automatically by directly converting voxels in image coordinates into meshfree points in physical coordinates that are embedded in a surface mesh representation of the image segmentation boundary. The novelty is that a one-to-one relationship between image data and meshfree model is established. This allows to directly map the model's solution to the image data and may aid the clinician during the simulation interpretation process.

II. METHODS

A. Mixed Collocation Method Monodomain Model

The monodomain model assumes equal anisotropy ratios for the intracellular and extracellular spaces. Under this assumption, the propagation of the electrical impulse is obtained by solving the reaction-diffusion equation:

$$\begin{aligned} &\partial V/\partial t = \boldsymbol{\nabla}\cdot(\boldsymbol{D}\boldsymbol{\nabla}V) - I_{ion}(V)/C && \text{in } \Omega \\ &\boldsymbol{n}\cdot(\boldsymbol{D}\boldsymbol{\nabla}V) = 0 && \text{on } \partial\Omega \end{aligned} \tag{1}$$

where V is the transmembrane potential, I_{ion} is the total ionic current and C is the cell capacitance per unit surface

Research supported by the European Research Council under grant agreement ERC-StG 638284, by the European Union's H2020 Program under grant agreement No. 874827 (BRAV3), by Ministerio de Ciencia e Innovación (Spain) through project PID2019-105674RB-I00 and by European Social Fund (EU) and Aragón Government through BSICoS group (T39_20R).

Konstantinos A. Mountris is a Research Fellow and the corresponding author in BSICoS group, University of Zaragoza, IIS Aragón and CIBER-BBN, Zaragoza, Spain. (Email: kmountris@unizar.es).

Manuel Doblaré is Full Professor in Tissue Microenvironment (TME) Lab. Aragón Institute of Engineering Research (I3A), University of Zaragoza and CIBER-BBN, Zaragoza, Spain. (Email: mdoblare@unizar.es).

Esther Pueyo is Associate Professor in BSICoS group, University of Zaragoza, IIS Aragón and CIBER-BBN, Zaragoza, Spain. (Email: epueyo@unizar.es).

area. Ω and $\partial\Omega$ denote the domain of interest and its boundary; $\boldsymbol{n}$ is the outward unit vector normal to the boundary; $\boldsymbol{D}$ is the diffusion tensor given by:

$$\boldsymbol{D} = d_l \left[(1-\rho)\boldsymbol{f} \otimes \boldsymbol{f} - \rho \boldsymbol{I}\right] \tag{2}$$

where d_l denotes the longitudinal diffusion coefficient, $\rho \leq 1$ is the transverse-to-longitudinal conductivity ratio and $\boldsymbol{f}$ is the cardiac fiber direction vector. $\boldsymbol{I}$ denotes the identity matrix and $\otimes$ the tensor product operation.

The Mixed Collocation Method (MCM) formulation of the monodomain model is derived applying operator splitting to decouple the reaction and diffusion terms in Equation (1). We construct the Petrov-Galerkin weak-form of the diffusion term's equation using meshfree approximants as approximation functions and the Dirac delta distibution as test functions. Applying interpolation to both V and $\boldsymbol{\nabla} V$ using the meshfree approximants, we obtain:

$$\begin{array}{ll} \partial V_i/\partial t = -I_{ion}(V_i)/C & \text{in } \Omega \\ \sum_{j=1}^{m} \phi_i^j \partial V_j/\partial t = \sum_{j=1}^{m} \boldsymbol{\nabla} \cdot \boldsymbol{D} \boldsymbol{\nabla}^T \phi_i^j V_j & \text{in } \Omega \\ \sum_{j=1}^{m} \boldsymbol{n} \cdot \boldsymbol{D} \boldsymbol{\nabla} \phi_i^j V_j = 0 & \text{in } \partial\Omega \end{array} \tag{3}$$

where $i = 1, 2, \ldots, n$ connotes the field nodes in the discretization of Ω, $j = 1, 2, \ldots, m$ connotes the field nodes in the support domain of i (being i one of these nodes) and ϕ_i^j is the value of the meshfree interpolation vector $\boldsymbol{\phi}_i$ for component j.

In this work, we use the Moving Kriging Interpolation (MKI) meshfree approximants, so $\boldsymbol{\phi}_i$ is then expressed as:

$$\boldsymbol{\phi}_i = \boldsymbol{p}_i \boldsymbol{A} + \boldsymbol{c}_i \boldsymbol{B} \tag{4}$$

where $\boldsymbol{p}_i$ denotes the linear polynomial basis vector

$$\boldsymbol{p}_i = [1 \; x_i \; y_i \; z_i] \tag{5}$$

with x_i, y_i, z_i being the spatial coordinates and $\boldsymbol{c}_i$ being the correlation function vector. We use Multiquadric Radial Basis Function (MQ-RBF) as correlation function to obtain:

$$\begin{aligned} \boldsymbol{c}_i &= [c_{i1} \; c_{i2} \; \ldots \; c_{im}] \\ c_{ij} &= \left(r_{ij}^2 + r_c^2\right)^q \\ r_c &= \alpha_c d_c \end{aligned} \tag{6}$$

where r_{ij} is the Euclidean distance between points i and j. r_c and q denote shape parameters. The matrices $\boldsymbol{A}$ and $\boldsymbol{B}$ are obtained by:

$$\begin{aligned} \boldsymbol{A} &= (\boldsymbol{P}^T \boldsymbol{C}^{-1} \boldsymbol{P})^{-1} \boldsymbol{P}^T \boldsymbol{C}^{-1} \\ \boldsymbol{B} &= \boldsymbol{C}^{-1} (\boldsymbol{I} - \boldsymbol{P}\boldsymbol{A}) \end{aligned} \tag{7}$$

where $\boldsymbol{P}$ and $\boldsymbol{C}$ are the moment matrices for the polynomial basis matrix and the correlation matrix, respectively.

B. Image-based model generation

The pipeline for image-based meshfree model generation for *in silico* electrophysiology is depicted in Figure 1. In the following, we describe the process to generate a biventricular model from *ex vivo* diffusion-weighted magnetic resonance imaging (DW-MRI) data of a porcine heart. The data was acquired at Instituto de Investigación Sanitaria Gregorio Marañón (IISGM) using Philips Achieva 1.5T.

1) Image segmentation: Ventricles of an *ex vivo* porcine heart were segmented manually from a DW-MRI dataset with dimensions $128 \times 128 \times 83$ and voxel size $1.09 \times 1.09 \times 1.2$ mm using 3DSlicer. Three different labels were included in the segmentation, partitioning the ventricular anatomy in endocardial:midmyocardial:epicardial regions with a 45:25:30 ratio. Median filter smoothing with 2mm kernel size was applied on the segmentation data to ensure a smooth boundary.

2) Meshfree model: The meshfree model was generated automatically from the segmentation data using the immersed grid approach. Meshfree field nodes were distributed at the center of each voxel belonging to the segmentation of the ventricular anatomy. Endo:mid:epi partition information stored in the segmentation data voxels was assigned to the meshfree field nodes. Subsequently, a smooth triangular surface mesh representation of the segmented ventricles was generated using Delaunay triangulation. The average triangle circumference of the mesh was 0.9 mm. An inclusion test [7] was performed to discard field nodes that were located outside of the triangular mesh boundaries. The final model was composed of the field nodes inside the triangular mesh and on its surface. The surface connectivity was discarded since it is not required for MCM.

3) Myocardial fibers: The direction of myocardial fibers for voxel-derived field nodes was computed by processing the DW-MRI data and computing diffusion tensor (DT) fields. Prior to DT computation, Linear Minimum Mean Squared Error (LMMSE) filtering using joint information was applied to reduce Rician noise [8]. DT fields were computed by first evaluating a tensor spline from a weighted intrinsic average of tensors using Riemannian distances and then minimizing the Riemannian distance between the evaluated tensor spline and the DW-MRI data [9]. Next, the eigenvalue problem was solved for each voxel's diffusion tensor field to obtain the principal eigenvector, which was considered as the direction of the cardiac fiber direction at the corresponding field nodes. The direction of cardiac fibers at field nodes on the surface of the triangular mesh was computed using interpolation with MKI approximants.

4) Conduction system: The conduction system of the biventricular anatomy was generated in two steps. Initially, the bundle of His was constructed manually by including field nodes laying on the endocardial surfaces of the two ventricles. The bundle of His branched into the left and right bundle branches, which conduct the electrical impulse to the left ventricle (LV) and the right ventricle (RV), respectively. The left bundle branch was further subdivided into left anterior and posterior fascicles. Next, a fractal tree algorithm was used to generate the Purkinje branches of

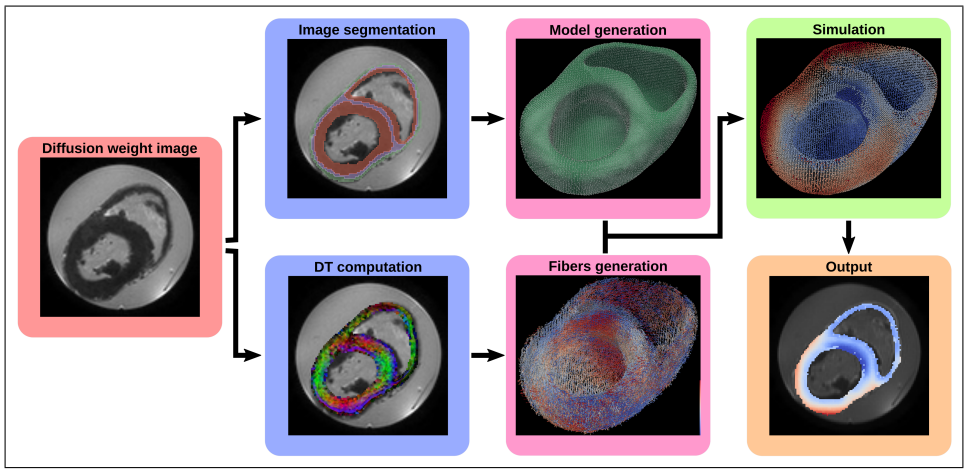

Fig. 1: Image-based model generation pipeline. All the tasks in the depicted process were performed automatically except for the segmentation task, which was performed manually.

the conduction system [10]. Purkinje-myocardial junctions (PMJ) were computed using a range-search algorithm to identify meshfree field nodes of the biventricular model that lie inside the sphere of influence (R=2mm) of each end-point of the Purkinje network.

C. MCM simulation & validation

A simulation of the electrical propagation in the biventricular model (field nodes: 70027) was performed using MCM with MKI approximants. MQ-RBF was chosen as correlation function for the MKI computation using shape parameters $r_c = 1.03$ and $q = 1.62$. Support domains were constructed including 160 nearest field nodes to ensure high collocation accuracy. Cell electrophysiology was described by the O'Hara model [11].

Rather than implementing electrical impulse propagation in the conduction system, PMJs were partitioned into seven groups: LV septum (LVS); LV base (LVB); LV mid (LVM); LV apex (LVA); RV base (RVB); RV mid (RVM); and RV apex (RVA). A time delay was applied during stimulation to obtain a realistic activation pattern [12]. The applied time delays at the different groups were $LVS = 0$ ms, $LVB = 25$ ms, $LVM = 14$ ms, $LVA = 5$ ms, $RVB = 27$ ms, $RVM = 16$ ms and $RVA = 7$ ms. The stimulus amplitude was twice the diastolic threshold, its duration was $t_d = 1$ ms and its period $t_p = 1$ s. Simulations were performed using a dual adaptive explicit time integration method with time step $dt = 0.1$ ms [13].

After achieving steady-state when pacing at a cycle length of 1000 ms, the electrical impulse propagation for $t = 500$ ms was simulated to measure the local activation time (LAT) and the action potential duration at 90% repolarization (APD_{90}). LAT was calculated as the time interval between the stimulus application ($t = 0$ ms) and the time instant of each AP's maximum upstroke derivative.

To validate the MCM solution, the same simulation was performed with FEM using a tetrahedral mesh (nodes: 44694, elements: 220084) of the biventricular anatomy. The endocardial, midmyocardial or epicardial attribute as well as the cardiac fiber direction were assigned to each node of the tetrahedral mesh identifying them with the corresponding values of the nearest meshfree field node.

III. RESULTS

LAT measurements in MCM and FEM simulations were in good agreement. For both simulations, LAT lied in the range $1 - 69$ ms. The mean LAT value was 25.54 ms for MCM and 25.38 ms for FEM. A comparison of normalized histograms for MCM and FEM is shown in Figure 2. As it can be observed from Figure 2, differences were mainly in the LAT range of $5 - 30$ ms, with more nodes in this range being activated for FEM as compared to MCM.

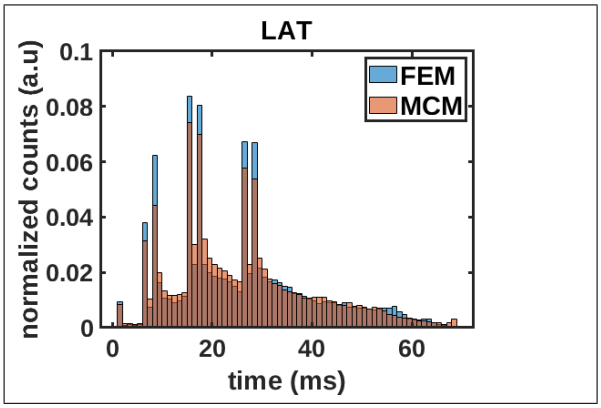

Fig. 2: Normalized histogram of LAT for FEM and MCM simulations.

Similar results were obtained for APD_{90}, which was in the range $180 - 285$ ms for both MCM and FEM. The APD_{90} average value was 249.46 ms for MCM and 248.80 ms for FEM. In the APD_{90} normalized histogram (Figure 3), the highest difference between MCM and FEM solutions is in the range $220 - 250$ ms, with more nodes having APD_{90} in this range for the FEM simulation. In addition, LAT and

APD_{90} differences between MCM and FEM were quantified by calculating the normalized histogram intersection (NHI) as a metric of histogram similarity ranging between 0 and 1. High similarity was found for both LAT and APD_{90} histograms with $NHI_{LAT} = 0.91$ and $NHI_{APD90} = 0.74$.

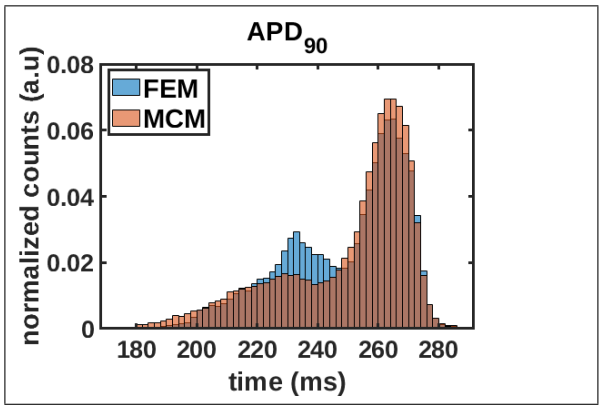

Fig. 3: Normalized histogram of APD_{90} for FEM and MCM simulations.

In terms of execution efficiency, the FEM simulation required 8.6 mins while the MCM simulation required 13.3 mins ($1.5\times$ slower). Finally, in Figure 4 we provide LAT and APD_{90} color maps generated by MCM in the voxel coordinates system since the one-to-one relationship between the field nodes of the image-based meshfree model with the voxels of the image data allows to interpret the MCM solution results directly on this coordinate system.

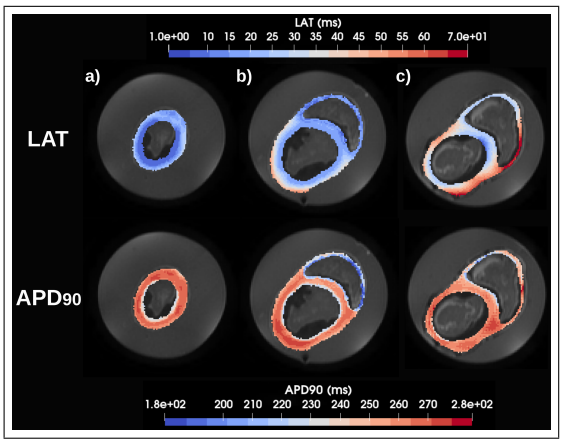

Fig. 4: LAT and APD_{90} color map interpretation in voxel coordinates system. Axial slice at a) $z = 18$ mm, b) $z = 36$ mm and c) $z = 61.2$ mm.

IV. DISCUSSION AND CONCLUSION

In this study, we present a novel approach for image-based meshfree model generation using the MCM method for *in silico* electrophysiology. We demonstrate that MCM can generate results in good agreement with FEM with minimum efficiency overhead.

The great advantage of MCM over FEM is that it alleviates the requirement of a good-quality mesh. Moreover, the proposed approach allows the automatic conversion of the image data to a meshfree model. This one-to-one relationship between the meshfree model's field nodes and the image data voxels allows for direct translation of the meshfree model's results to the image coordinates without requiring any type of interpolation. Therefore, this action is free of any interpolation-related error.

We believe that this approach may provide additional value to *in silico* electrophysiology, especially for clinical applications, since it does not require any feedback from the user during the model generation and the simulation process. Furthermore, it allows to associate simulation results with image data heterogeneity as well as to interpret the results directly on the medical image data, thus representing a highly convenient approach to be used by physicians.

ACKNOWLEDGMENT

We thank Ph.D. Pablo Martinez-Legazpi and M.D. Francisco Fernández-Avilés at Instituto de Investigación Sanitaria Gregorio Marañón for providing the DW-MRI dataset.

REFERENCES

[1] L. Tung, A bi-domain model for describing ischemic myocardial dc potentials (Doctoral dissertation), Massachusetts Institute of Technology, 1978.
[2] J.P. Keener, and J. Sneyd, Mathematical physiology, vol. 1, New York: Springer.
[3] H. Zhang, H. Ye, and W. Huang, A meshfree method for simulating myocardial electrical activity, Computational and mathematical methods in medicine, 2012.
[4] K.A Mountris, C. Sanchez, and E. Pueyo, A novel paradigm for in silico simulation of cardiac electrophysiology through the Mixed Collocation Meshless Petrov-Galerkin Method, In 2019 Computing in Cardiology (CinC), IEEE, pp.1-4, 2019.
[5] K.A Mountris and E. Pueyo, The radial point interpolation mixed collocation method for the solution of transient diffusion problems, Engineering Analysis with Boundary Elements, 121, pp.207-216, 2020.
[6] K.A Mountris and E. Pueyo, Next-generation in-silico cardiac electrophysiology through immersed grid meshfree modelling. Application to simulation of myocardial infarction, In 2020 Computing in Cardiology (CinC), IEEE, pp.1-4, 2020.
[7] J. Liu, Y.Q. Chen, J.M. Maisog, and G. Luta, A new point containment test algorithm based on preprocessing and determining triangles, Computer-Aided Design, 42(12), pp.1143-1150, 2010.
[8] A. Tristan-Vega and S. Aja-Fernandez, DWI filtering using joint information for DTI and HARDI, Medical Image Analysis, 14(2), pp.205-218, 2010.
[9] A. Barmpoutis and B.C. Vemuri, A Unified Framework for Estimating Diffusion Tensors of any order with Symmetric Positive-Definite Constraints, In 2010 IEEE international symposium on biomedical imaging: from nano to macro (pp. 1385-1388). IEEE, 2010.
[10] F.S. Costabal, D.E Hurtado, and E. Kuhl, Generating Purkinje networks in the human heart, Journal of biomechanics, 49(12), pp.2455-2465, 2016.
[11] T. O'Hara, L. Virág, A. Varró and Y. Rudy, Simulation of the undiseased human cardiac ventricular action potential: model formulation and experimental validation, PLoS Computational Biology, 7(5), p.e1002061, 2011.
[12] D. Durrer, R.T. Van Dam, G.E. Freud, M.J. Janse, F.L. Meijler and R.C. Arzbaecher, Total excitation of the isolated human heart. Circulation, 41(6), pp.899-912, 1970.
[13] K.A. Mountris and E. Pueyo, A dual adaptive explicit time integration algorithm for efficiently solving the cardiac monodomain equation, arXiv preprint, arXiv:2011.04747, 2020.